Polymer 50 (2009) 5434–5442

Contents lists available at ScienceDirect

Polymer

journal homepage: www.elsevier.com/locate/polymer

Particle-induced network formation in linear PDMS filled with silica

Anca Şerbescu [a,1], Kay Saalwächter [b,*]

[a] Institut für Makromolekulare Chemie, Universität Freiburg, Stefan-Meier-Str. 31, D-79104 Freiburg, Germany
[b] Institut für Physik – NMR, Martin-Luther-Universität Halle-Wittenberg, Betty-Heimann-Str. 7, D-06120 Halle, Germany

ARTICLE INFO

Article history:
Received 4 August 2009
Received in revised form
19 September 2009
Accepted 21 September 2009
Available online 27 September 2009

Keywords:
Nuclear magnetic resonance
Siloxanes
Gelation

ABSTRACT

We study the formation of permanent elastomers from linear PDMS chains by solution blending with up to 25 wt% fumed silica. The physical networks are characterized by time-domain multiple-quantum NMR. Based upon dynamic parameters measured for the linear precursor polymer, we develop a reliable strategy for component separation in this complex heterogeneous system, providing information on the amount of monomers involved in network-like material, in elastically inactive yet entangled linear chains, and isotropically mobile chain ends, as well as on the effective network chain length as measured via the average residual dipolar coupling constant. The use of untreated silica leads to permanent networks, for which the NMR results correlate well with macroscopic determinations of the relaxed Young modulus and the degree of swelling. Surface-modified silicas do not lead to percolated network structures, but still lead to the formation of 20–40% network-like material, with effective network chain lengths that depend on the surface functionalization and thus on the nanoparticle dispersion. Characteristic changes in the mobile chain end fraction with temperature, in particular its decrease with increasing degree of filling are interpreted as a consequence of altered contour-length fluctuations. An aging experiment conducted on a sample prepared by melt blending reveals the microscopic changes in the network structure occurring over many months.

1. Introduction

Silica particles are abundantly used as reinforcing agent for silicone elastomers [1], most prominently poly(dimethyl siloxane), PDMS, leading to advanced materials that are applicable even in high-precision applications such as microcontact printing [2]. The beneficial action of precipitated or, more popularly, fumed silica on PDMS is based upon the existence of strong multiple hydrogen bonds between surface–OH groups of the silica and the PDMS main chain [3], leading to a solid-like layer of 1–2 nm thickness irrespective of the PDMS end-group or whether the chains are grafted or just adsorbed [4–6]. The strength of the adsorption layer and thus the overall reinforcement effect in the composites was shown to decrease with an increase of surface water content [7,8], and along the same lines, silanization of the silica to render it more hydrophobic was demonstrated to decrease its affinity towards PDMS and other fluids capable of forming hydrogen bonds [9–11], thus also reducing the reinforcement observed for PDMS composites [10,12].

Chains participating in the adsorbed layer and extending well into the bulk melt, possibly bridging different particles [13] or additionally participating in trapped entanglements, are responsible for the fact that a large part of the PDMS, much more than the comparably small fraction present in the adsorption layer, is dynamically constrained, as directly evidenced by NMR [10,14]. The presence of such polymer bridges was assumed to be the reason for the large viscosity increase of lowly (~3 wt%) filled PDMS fluids [15], and was more directly proven by the observation that highly filled composites (>10 wt% silica) are in fact permanent networks with well-defined equilibrium degrees of swelling [9,16,17]. This can only be explained by the dominance of entropic elasticity, exerted by chains that connect silica particles acting as multifunctional crosslinks.

Such highly filled PDMS composites, which are most commonly prepared by melt blending, exhibit a complex rheological behavior [12,18–21], prominently shear thinning (Payne effect) related to strain-induced rearrangements in the filler network [12], and aging phenomena, also related to changes in the filler network with time [18,19]. The latter phenomenon is believed to be mainly due to a slow saturation of the silica surface with PDMS, replacing direct filler-filler contacts by polymer bridges, explaining a decrease in storage modulus with time.

It is the purpose of this paper to study the entropic network formation in more quantitative detail, providing information on the

* Corresponding author.
E-mail address: kay.saalwaechter@physik.uni-halle.de (K. Saalwächter).
URL: http://www.physik.uni-halle.de/nmr
[1] Present address. Dow Europe GmbH, Horgen, Switzerland.

0032-3861/$ – see front matter © 2009 Elsevier Ltd. All rights reserved.
doi:10.1016/j.polymer.2009.09.063

length of the network chains and heterogeneities in such elastomeric composites. Most of the valuable molecular-scale insights into the origin of the reinforcement effect in PDMS-silica composites have been obtained by proton NMR spectroscopy [10,14,22], where up to now the information content was limited to the amount of different components with qualitatively different transverse relaxation behavior, the latter depending on both the timescale of molecular mobility and, more prominently, on residual dipolar couplings that arise from the anisotropy of segmental motion as constrained by crosslinks and entanglement-type effects [10,23].

More advanced fits to such relaxation data in order to obtain quantitative information beyond average T_2 relaxation times and component fractions are subject to artifacts arising from the incomplete knowledge of the shape of the actual relaxation function [24], calling for more sophisticated NMR approaches in order to gain even more quantitative insights, for instance on the separation of entanglement effects from permanent crosslinks, and elucidating heterogeneities. As an example, NMR imaging work on PDMS elastomers with in-situ precipitated silica have indicated substantial spatial heterogeneity on a macroscopic (0.1 mm) scale [25]. Our recent work has demonstrated that proton multiple-quantum (MQ) NMR provides more quantitative information by virtue of a direct and model-free measurement of residual dipolar couplings, allowing for quantitative conclusions on the cross-link density (as detected locally), its distribution across the sample (thus any heterogeneity on the scale of a few nm and above), and about timescales of chain motion [26].

In applying MQ NMR methods to linear PDMS as crosslinked by physical bonds to fumed silica particles via a solution blending process, we obtain new insights which were previously inaccessible by the traditional combination of solvent-extraction techniques and NMR transverse relaxation. We study exclusively unextracted composites, so as to learn about the particle-induced network effects in typical bulk samples. We also characterize our samples by equilibrium swelling and mechanical experiments, the latter focussed at measuring the relaxed Young modulus at very small strains, which in contrast to dynamic (plateau) moduli is found to be governed by entropic elasticity rather than the filler network [18–20].

2. Experimental

2.1. Samples

The investigated base polymer (termed "Lin90k") was an alkyl-terminated PDMS obtained from Wacker Silicones ($M_n = 90$ kDa, $M_w = 128$ kDa, $PD = 1.43$). It was filled with 5–25 wt% of different fumed silicas in steps of 5%, corresponding to volume fractions ϕ_{sil} of about 3–15%. Both the polymer and the silica were first separately dissolved/dispersed in dried and freshly distilled toluene (Fluka) at 0.5 and 0.033 g/mL, respectively. The clear solutions were combined and left to stir at ambient temperature for 15 h. Note that adsorption of PDMS onto silica from solution is usually complete within a few hours [27]. After drying, the composites were placed in a vacuum oven and dried for 48 h at 363 K and 800 mbar. The samples were investigated repeatedly over several months, and showed no indications of the strong aging effects that are typically observed for composites obtained by melt processing.

As fillers, we used untreated Cabosil M5 fumed silica (Cabot), which consists of primary particles in the 10 nm range, present as aggregates of 200–300 nm size, with a BET area of around 200 m^2/g. The series is denoted "X-*f*", where *f* is the silica fraction in wt%. We compare this series with composites with two surface-modified versions, namely Cabosil TS-530 (trimethylsilyl-functionalized, 220 m^2/g) and Cabosil TS-720 (PDMS-oligomer-functionalized, 120 m^2/g), denoted "A-*f*" and "B-*f*", respectively. Surface-modified silica exhibits much reduced content of surface–OH groups, and therefore less adsorption sites to the PDMS.

The glass transition temperatures (temperature at which Δc_p reaches 50%) of the bulk composite samples were determined by DSC at 9 K/min. The data showed rather large statistical scatter for the samples filled to different degrees, which is why we report an average value. T_g varied characteristically for the different filler systems: Lin90k 141K; X 154 ± 3 K; A 147 ± 4 K; B 151 ± 3 K. These values give a crude indication of the overall immobilization efficiency of the different filler systems, identifying M5 (X) as most active filler, and TS-720 (B) as the next in the series.

At 10 wt% filling and above, the samples were slightly opaque, and the X series gave shape-persistent elastic gels, as illustrated in Fig. 1a. Fig. 1b–d show cryo-TEM images of the composites. They indicate substantial heterogeneity in all cases, i.e., the presence of larger agglomerates in combination with (b) small agglomerates and primary particles for X-15, (c) and (d) larger, more compact aggregates for A-15 and B-15, where in the latter case, also the agglomerates appeared more compact, which can in all cases be attributed to the different surface treatments.

^1H MQ NMR experiments were performed on a Bruker minispec mq20 ($B_0 = 0.5$ T) and evaluated following previously published procedures [26,28,29]. The sample temperature was maintained using a regulated airflow and varied between 250 and 300 K.

Swelling experiments were performed in toluene at 298 K, resulting in information on the effective crosslinking density. The volume degree of swelling was determined using a Will-Strübin (Wetzlar) optical microscope. The sample weight before and after swelling (including renewal of the excess solvent) was measured with a Mettler AT250 balance after drying in vacuum at room temperature, and used to determine the content of soluble material f_{sol}. From this, we calculated the effective degree of swelling $Q = 1 + V_{tol}/V_{net}$, which is related only to the (unextracted) network fraction, also assuming that the filler is unswellable and not part of the network. These experiments were performed on samples X-10 to X-25, which could be swollen to an equilibrium within 24 h and then retained constant volume, while all other samples did not remain structurally intact.

Stress–strain measurements were performed with a home-built device. In a thermostatic cell controlled by a Haake-F6 thermostat and equipped with a Pt100 thermocouple, the sample was stretched by an Owis SM400 microstep motor and controlled by an Owis SMK01 microstep controller. The stress was measured by a HBM PW4FC3 transducer load cell and analysed by an HBM KW3073 high performance strain gage indicator. All relevant data such as temperature, uniaxial strain, and uniaxial stress were continuously logged. A personal computer controlled the deformation stepwise, as specified by a script file. After each deformation step, the static response to the deformation, the uniaxial stress, was recorded when equilibrium was reached according to the slope and the standard deviation of the continuously logged data. Therefore below, we report the relaxed stress after each strain step as a function of strain.

3. Results and discussion

3.1. Strategies for signal component decomposition

The main challenge posed by the analysis of the bulk NMR response of a system as complex as the present ones is to pay proper reference to the heterogeneous nature of the response. While signal functions may be developed for idealized and hardly realizable systems such as defect-free end-linked model networks without polydispersity, it must be kept in mind that such

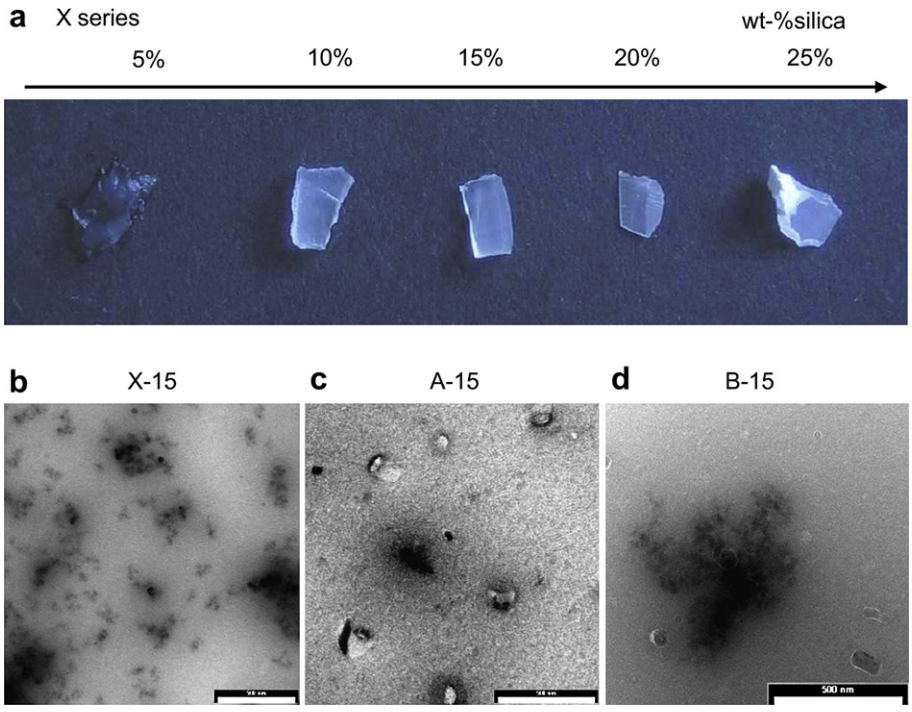

Fig. 1. (a) Appearance of the PDMS-silica composite samples (X series, with Cabosil M5) (b)–(d) Transmission electron micrographs of the samples with 15 wt% filler. The scale bars correspond to 500 nm.

a theoretical fitting function is subject to limitations when it is applied to a system that does not meet the requirements [24]. Therefore, fits must be restricted to a minimum number of free parameters, either using robust functions with fewer parameters, for instance based on reasonable assumptions such as a certain distribution shapes, or determining some parameters independently.

We follow both strategies, and start with the analysis of the NMR response of the linear precursor polymer. In the ensuing analysis of the composites, we assume that these samples still contain a certain fraction of linear precursor chains with the same (fixed) relaxation parameters, restricting the component analysis to just the amplitudes.

The MQ experiment yields two signal functions as a function of the MQ pulse sequence (evolution) time τ_{DQ}, the decaying sum MQ intensity (ΣMQ) and the double-quantum (DQ) build-up intensity, also subject to relaxation effects at longer times. Previous work [30] has shown that the ΣMQ decay is dominated just by the timescale of segmental orientation fluctuations, while the DQ build-up is governed by residual dipolar couplings (D_{res}), related to entanglement as well as cross-link effects rendering the motion anisotropic on the ms timescale. D_{res} is our major observable, as it is directly proportional to cross-link density [31]. The decay of the DQ signal at longer times is more complex and depends on faster segmental modes as well as slower chain modes (reptation) in case of linear melts. It was also found that these effects are approximately multiplicative, i.e., a point-by-point division of the DQ signal by the ΣMQ decay yields a normalized DQ (nDQ) build-up function that in a network depends exclusively on D_{res}, and it relaxes only in non-network samples when slower chain modes (reptation and the like) are present [32]. Therefore, the nDQ intensity function is temperature-independent in permanent networks.

Before calculation of the nDQ intensity by division, slowly relaxing singly exponential tails must be subtracted from the sum intensity. These represent contributions from segments involved in fast isotropic motion, most prominently from chain ends (or network defects) that are not subject to tube/entanglement constraints and move isotropically on a timescale of the entanglement time τ_e. Their relative amount depends on molecular weight and temperature. Such components have previously been interpreted as a result of contour-length fluctuation processes [33,34]. Fig. 2a and Table 1 show the results of this decomposition. Singly exponential fits were performed on ΣMQ data for times >60 ms, which is a stable procedure as the $T_{2,\,tail}$ is at least a factor of 3 longer than the decay due to the chain centers.

After subtraction, the nDQ intensity is calculated and analyzed according to [26,35]

$$I_{nDQ}(\tau_{DQ}) = \int_0^\infty \frac{1}{2}\left(1 - \exp\left\{-\frac{2}{5}D_{res}^2\tau_{DQ}^2\right\}\right) \times P(D_{res}) \exp\left\{-\frac{\tau_{DQ}}{T_2^*}\right\} dD_{res}, \quad (1)$$

where a gamma distribution function of couplings [28],

$$P(D_{res}) = \frac{2}{\sqrt{\pi}}\sqrt{\frac{27\,|D_{res}|}{8\,\overline{D}_{res}^3}}\, e^{-3\,|D_{res}|/(2\,\overline{D}_{res})} \quad (2)$$

was used. The distribution integral was evaluated numerically using finite differences as a part of the fitting protocol. The fits were iteratively constrained to $\tau_{DQ}^{max} = 2.4/\overline{D}_{res}$, as this is the approximate validity limit for the build-up Kernel function in Eq (1) [30]. Fits using a single value for $\overline{D}_{res}$ (no distribution), that work very well in elastomers, provide only poor representations of the data, as a result of the complex effect of reptation dynamics on I_{nDQ}, for which at present no closed-form analytical expression exists. The gamma distribution has some physical relevance, as it is expected on the basis of single-chain models that assume a Gaussian end-to-end distribution between entanglement constraints in a monodisperse system [36]. Its advantage here is that its width is related to the average $\overline{D}_{res}$, such that no additional parameter is introduced

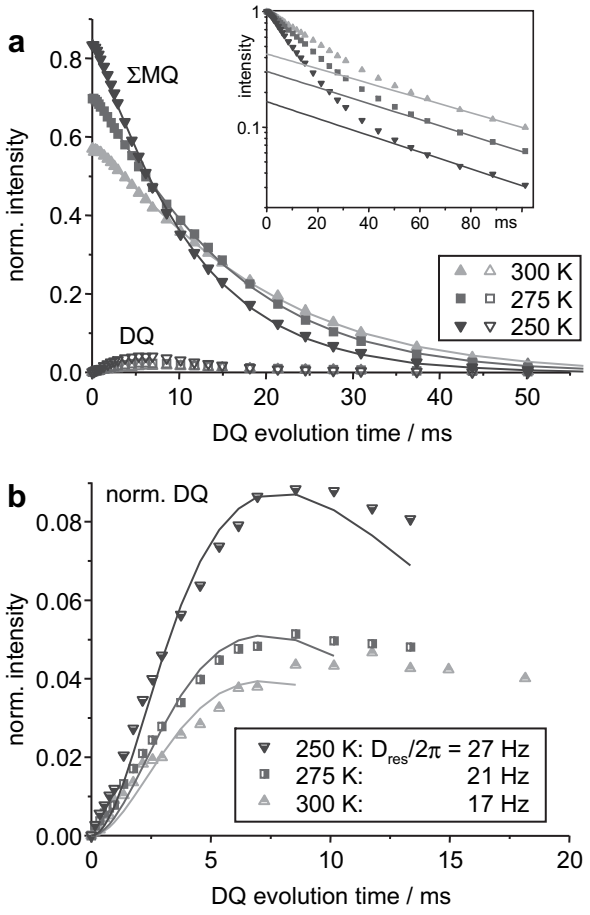

Fig. 2. MQ NMR data for the linear precursor polymer Lin90k. (a) Raw data for the DQ build-up intensity and the sum MQ intensity (ΣMQ). The latter is corrected by subtraction of slowly relaxing tail fractions related to chain ends, shown as lines in the inset. (b) Normalized DQ intensity obtained by division of the DQ and ΣMQ data, along with fits to Eq (1).

and a stable fitting result is obtained. The overall intensity build-up is well-described by the two-parameter fit (Fig. 2b), while the deviation at very short and long times merely reflect the qualitative nature of the crude model and its inability to properly account for reptation dynamics. An improved approach will be reported shortly. Here, the combined entanglement/reptation effects are characterized by an apparent T_2^*, which varies only weakly between 6 and 9 ms, and the average $\overline{D}_{res}$ given in Table 1. The latter represents the chain orientation due to non-relaxed entanglements on the ms timescale.

These results are merely meant to highlight the phenomenology of MQ signals in polymer melts, the quantitative analysis of which is a matter of ongoing work. For the subsequent analysis of the composites, we primarily focus on the ΣMQ relaxation functions. We found that the linear melt data as well as, generally, all signal decays observed in very different types of networks, PDMS, natural rubber, etc. [26,28,30], are almost perfectly fitted by a combination of one exponential (for the tail fraction) and a Weibullian function,

$$I_{\Sigma MQ} = f_{tail}\exp\{-\tau_{DQ}/T_{2,tail}\} + f_{ctr}\exp\{-(\tau_{DQ}/T_{2,ctr})^{\beta}\} \quad (3)$$

The fitting results for the Lin90k are again listed in Table 2.

In the following, we assume that the signal functions of the composite samples, examples of which are shown in Fig. 3, can be modeled by a superposition of (i) a melt-like chain end fraction, (ii) melt-like center fraction, and (iii) a network fraction. Further, based upon the observation that the ΣMQ intensity decay associated with even moderately crosslinked (entanglement-dominated) networks is 99% complete within 20 ms, we determine all fractions in the composites by fitting Eq (3) to the tails of the composite signals starting at 20 ms, keeping the relaxation parameters (T_2, β) fixed for the given temperature. A back extrapolation directly gives f_{tail}, f_{ctr}, and f_{net}.

Table 1
Relaxation parameters for the Lin90k sample.

T, K	tails, %	$T_{2,\,tail}$, ms	$T_{2,\,ctr}$, ms	β	$\overline{D}_{res}/2\pi$, Hz
300	0.43	68.4	19.5	1.19	17
275	0.30	63.0	16.0	1.15	21
250	0.17	59.7	11.6	1.10	27

The final step is the closer characterization of the network fraction. For this, it must be noted that the overall DQ build-up is a superposition from the network and the linear-chain center fraction, where the former actually dominates the latter. We therefore subtract an interpolation of the experimental linear-chain DQ build-up curves (Fig. 2a), weighted by f_{ctr} obtained from the fit to $I_{\Sigma MQ}$, from the DQ build-up measured for the composite. The results (DQ corr. in Fig. 3) are characteristic for the network fraction, and can be normalized (point-by-point division) by the corresponding $I_{\Sigma MQ}$, also corrected by subtraction of Eq (3). The resulting nDQ curves should be temperature-independent, and they characterize the average crosslink density of the network fraction.

The feasibility of our approach is demonstrated in Fig. 3, where so-obtained nDQ build-up curves are compared with nDQ build-up curves that were obtained in the usual way as in conventional elastomers [26,37], where two singly exponential tail fractions f_{tail} and f_{ctr} with freely fitted relaxation times were considered, and the DQ signal was not corrected. This strategy of course lead to systematic deviations in the fractions and the corresponding T_2 times, but the good correspondence of the resulting nDQ curves demonstrates that the network fraction is indeed reliably extracted by both strategies. However, we point out that the approach with the fixed melt-based parameters provided clearer trends and less scatter, in particular for the surface-modified systems with their low network fractions. Also note that an overall stable component decomposition is crucially based upon a good separation of the different relaxation times, which in our case are all at least a factor of ~3 apart. We estimate possible systematic errors for all fractions to around ±10%. The scatter and systematic deviations observed for nDQ at longer times in excess of 10 ms is mainly due to the almost complete relaxation of the sum signal, which amplifies the small absolute-scale errors of the also rather small DQ intensity upon normalization.

The nDQ curves for the network fractions could in all cases not be described by a single-component build-up function that is usually applicable for homogeneous single-component networks, but exhibited indications of a substantial distribution

Table 2
Results from swelling and mechanical experiments for the X series, compared to NMR parameters (see Fig. 4).

sample	Q	f_{sol}	E_r/MPa	$D_{res}/2\pi$/Hz[a]	f_{net}[a]
X-10	6.7	0.62	0.15	111 ± 5	0.43 ± 0.02
X-15	4.8	0.58	1.41	209 ± 12	0.42 ± 0.02
X-20	4.0	0.55	2.53	163 ± 16	0.65 ± 0.08
X-25	3.3	0.51	–	206 ± 10	0.76 ± 0.03

[a] NMR results and error margins are from averages over the different experimental temperatures.

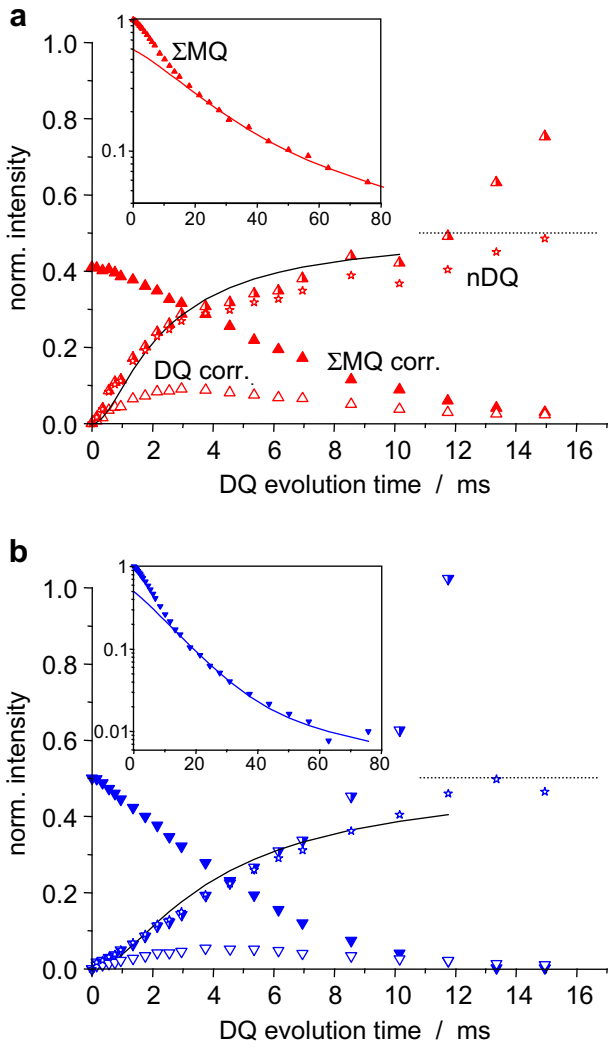

Fig. 3. Data illustrating the component decomposition for the samples (a) A-25 at 250 K and (b) X-10 at 300 K. Full and open triangles are corrected data corresponding to the overall signal functions $I_{\Sigma MQ}$ and I_{DQ}, respectively, after subtraction of the melt-like parts, and half triangles are normalized DQ build-up curves, (I_{nDQ}) characterizing the network-like component. Stars are corresponding curves for normalization after a conventional bi-exponential tail subtraction from $I_{\Sigma MQ}$ with free parameters. Solid lines are fits to determined $\overline{D}_{res}$ and the dotted lines indicated the expected 50% intensity plateau. The insets show the full $I_{\Sigma MQ}$ decay functions and the fits to Eq (3) for the determination of the melt-like fractions (tails and chain centers).

(heterogeneity), as discussed in our first publication on the topic [28]. Since the data are quite noisy for cases with low f_{net}, we refrained from a closer analysis of the cross-link density distribution, and used Eq (1) for $T_2^* \to \infty$ as a fitting function. We thus impose the assumption of a gamma distribution of D_{res}, which has the advantage of not introducing another fitting parameter (the width is related to the average of this distribution). While for the case of the single-component response of a linear melt, this was meant to provide a stable fit for a function whose shape is not known exactly, it here is a means to obtain a well-defined average $\overline{D}_{res}$ over the signal of a truly heterogeneous sample.

3.2. Comparison of composites with different surface treatments

We are now in a position to discuss the results of our component analysis, which are summarized in Fig. 4. Let's first consider the network fractions (crossed symbols in the lower panel). As expected, the amount of network material is highest in the untreated X series, and reaches up to 80% for 25 wt% silica. Therefore, direct particle-particle bridges, or at least topologically linked loop structures must be present for most of the polymer chains. This is possible because of the good filler dispersion, where apart from agglomerates, smaller isolated particles or small clusters must be dispersed throughout the matrix with distances on the order of the radius of gyration of the polymer (~ 10 nm). The TEM observations for sample X-15 in Fig. 1b is compatible with this scenario. Note that samples with 10 wt% and more silica are elastomers with a percolated network structure.

The trimethylsilyl-modified series has network fractions only up to 40%, and the PDMS-modified series reaches just above 10%, and none of these samples form permanent networks, meaning that the network fraction does not form a percolated substructure. Apart from statistical scatter, in all systems, we do not observe a systematic temperature dependence, neither in f_{net} nor in the $\overline{D}_{res}$, see the upper panel. This indicates a successful component analysis, as the physical bonds forming the network are not expected to weaken dramatically in the studied temperature range. It is interesting to observe that in both the A and B series, the residual coupling characterizing the (inverse) typical network chain length is almost constant, while it rises monotonically in the X series. We interpret the constant values with different silica densities in agglomerates of rather concentration-independent size, which are more compact for the B series (PDMS functionalization), see also Fig. 1d. This leads to shorter chain bridges and thus higher $\overline{D}_{res}$. Note that crosslinks in the B series can only be formed by penetration of matrix chains into the glassy adsorbtion layer that is already present through the PDMS functionalization [13], blocking most of the surface. Judging from the low network fractions, this is not a very efficient binding mode. In contrast, bonds between A-type particles only form via hydrogen bonds to residual surface–OH groups.

In contrast, the X series exhibits not only increasing network fractions, but also a gradually decreasing network chain length, which means that the particle distributions changes with filling. Note that the X-15 sample, which falls slightly besides the trend, probably has a somewhat more compact agglomerate structure (smaller f_{net}, higher $\overline{D}_{res}$), possibly due to variations in the preparation conditions. However in summary, the effective (volume-averaged) elasticity modulus of this sample (see below) follows the expected trend.

Turning to the f_{tail} and f_{ctr} components, we do observe characteristic changes with temperature in all cases. Essentially, higher temperatures lead to an increasing chain end fraction f_{tail} and a faster associated relaxation time, and a correspondingly decreasing f_{ctr}, which is a typical consequence of contour-length fluctuations. It is interesting to observe that increasing filling in all cases leads to a substantial decrease of the tail fraction, while the center fraction does not necessarily decrease in parallel, which would be expected on the basis of a 1:1 conversion of free chains into network chains. We interpret this as a consequence of altered chain dynamics and contour-length fluctuation mechanisms. When a given chain is adsorbed at some point along its contour, it is of the center- rather than network-type, as it is not fixed at two ends and does not exhibit a temperature-independent residual coupling, yet the ends still undergo isotropic motions (tail-type). However, the effective length of this freely moving tail is much reduced due to the inability to perform reptation motion. Such observations are of much significance in the context of understanding the influence of contour-length fluctuations on rheological properties of polymer melts [38,39], and corresponding NMR studies on models such as networks with controlled amount of dangling ends or linear melts

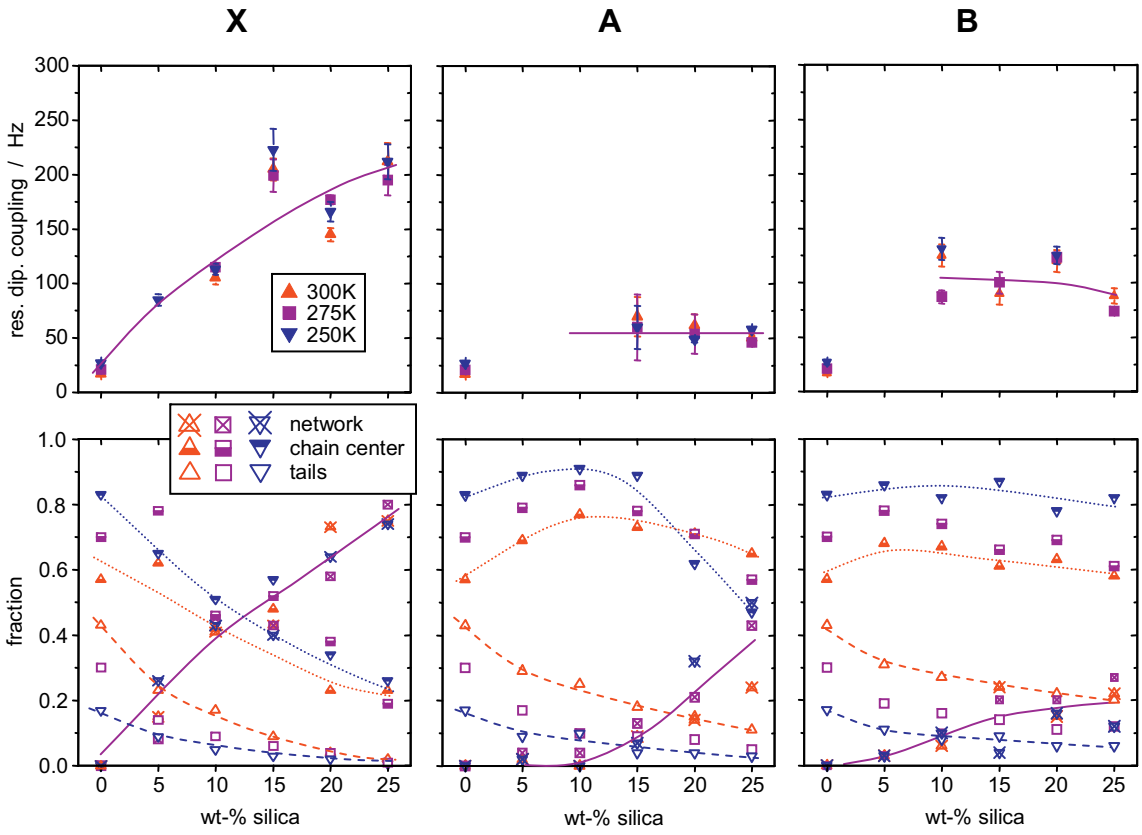

Fig. 4. Results for the component analysis (bottom) and the characterization of the network-like part (top) for all samples. All lines are guides to the eye indicating the trends for the chain end fraction (dashed lines), chain center fraction (dotted) and network-like parts (solid). For the former two cases, the two lines each mark the trends within the investigated temperature range.

with isotope-labelled end blocks are currently being performed by us and others [34,40].

3.3. Correlation with macroscopic properties

We now focus again on the X series, for which the NMR results can be used to predict the trend for the elasticity modulus under the assumption of pure entropic elasticity. The residual coupling is inversely related to the number of segments per network chain, which in turn is proportional to the inverse network chain molecular weight, and thus the cross-link density, $D_{res} \propto 1/N \propto 1/M_c \propto \nu_c$. In order to predict the modulus $E \propto \nu_c$, one needs to take into account that not all PDMS monomers in the given sample volume belong to network chains, which is why the result must be multiplied by the (NMR-determined) network fraction of the bulk sample f_{net}. Thus, $E \propto D_{res} f_{net}$. Finally, assuming only hydrodynamic filler effects and neglecting a potential filler network, the contribution due to passive high-modulus silica particles is taken into account by a modified Einstein relation (initially proposed for the viscosity of a dilute particle suspension), as generalized for the modulus of more highly filled elastomers by Guth and Gold [41], $E_{filled} = E_{matrix}(1 + 2.5\phi_{sil} + 14.1\phi_{sil}^2)$.

Results from the mechanical experiments are shown in Fig. 5a. We remind that each point of the stress–strain curves is measured in the relaxed state after thorough equilibration (see Experimental). Note also that the experiments were performed for very small strains, for which we are confident that the results can be used to extract E in the linear regime. Only three samples could be measured, as X-5 did not form a permanent network, and X-25 was too brittle to be mounted in our apparatus. The samples X-10 and X-15 exhibit the shear thinning behavior usually found for filled systems [12], while initial shear thickening is observed for X-20. This peculiar behavior may be interpreted as the onset of a jammed filler-filler network. Note that this effect may have as yet been overlooked, as most rheological studies are limited to larger strain and non-relaxed stress measured at a given strain rate (thus being dominated by filler-filler network effects even at the smallest strains), and modulus and stress are often discussed on a logarithmic scale. The phenomenon clearly deserves further exploration. For the given purpose, we assume that our E_r as estimated from the initial slope is dominated by the entropic elasticity of the PDMS chains bridging the particles.

Results from the mechanical experiments, along with the NMR data needed for comparison and the results from the equilibrium swelling experiments are collected in Table 2. According to Flory [41], the crosslink density of a rubber scales as $Q^{-5/3}$ for high degrees of swelling, and we plot this quantity as well as the experimental E_r vs. the NMR-predicted modulus (in units of D_{res}) in Fig. 5b. Within the uncertainty set by the limited set of data, both comparisons reveal the expected linear scaling, suggesting that the mechanical properties of the composites in the relaxed state are indeed dominated by entropy elasticity.

The NMR-mechanical correlation gives a residual coupling of ~50 Hz for a system with zero relaxed modulus (=linear melt), and this value is in the range observed for highly entangled linear chains, where the experimental D_{res} is then dominated by $1/M_e$ [31], see also Fig. 2 (NMR generally measures the unrelaxed modulus). In addition, the range of moduli observed for the composites and the corresponding effective NMR values for the modulus given as effective D_{res} (x-axis in Fig. 5b) are in good agreement with results

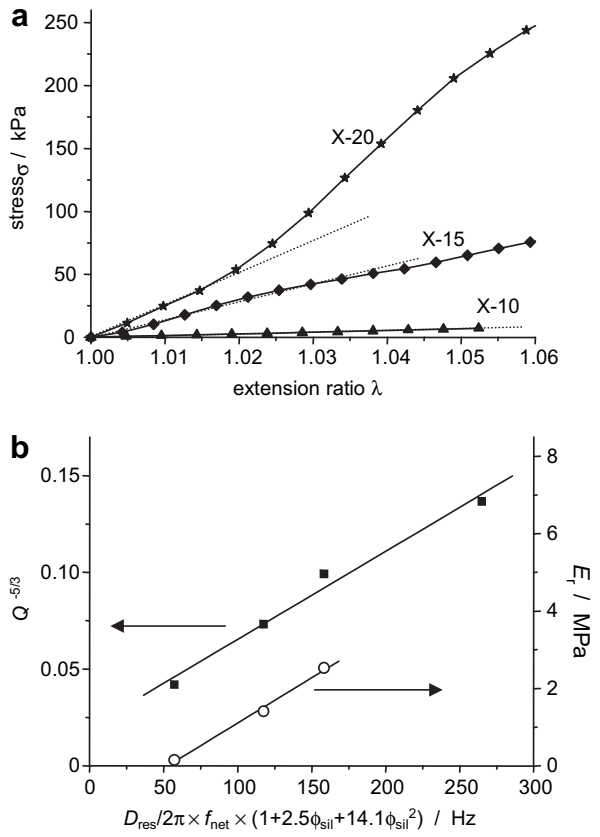

Fig. 5. (a) Fully relaxed stress–strain curves for three X samples, with dotted lines indicating the linear fits to determine the relaxed Young modulus E_r. (b) Correlation of E_r and the effective crosslink density of the swollen and extracted samples $\propto Q^{5/3}$ with the NMR-determined crosslink density. Note that for $f_{net}=1$ and $\phi_{sil}=0$, the latter quantity reflects the D_{res} of an unfilled bulk network sample without defects.

previously obtained for homogeneous PDMS model networks with M_c in the range of 5–100 kg/mol [28]. Note that this limiting case is recovered for $f_{net}=1$ and $\phi_{sil}=0$. The observed moduli may be compared with the entanglement-level (plateau) modulus at about 0.1 MPa [42], which means that sample X-10 (with $G \approx E/3 \approx 0.05$ MPa) has a crosslink density with an average cross-link spacing much larger than M_e, which is roughly 12 kg/mol, noting again that 60% of its volume consists of elastically inactive linear or dangling chains.

The swelling-NMR correlation roughly extrapolates to the origin, while it would be expected to extrapolate to the same D_{res} for infinite swelling (zero $Q^{-5/3}$). This would directly correspond to the expected behavior of infinite swelling for a sample with zero E_r. For a possible explanation one has to keep in mind that the $Q^{-5/3}$ vs. D_{res} correlation must be interpreted with care, since the samples change upon swelling, as is evident from Table 2. In particular for higher silica content, the extractable sol fraction f_{sol} becomes larger than $1-f_{net}$ determined by NMR, which means that upon swelling some chains are dissolved that are initially bound and behave as part of the elastic matrix in the bulk composite. This highlights the limited value of bound-rubber determinations, usually performed by exhaustive extraction and centrifugation, for the prediction of mechanical properties of filled elastomers, and stresses the value of molecular-scale in-situ investigations.

3.4. Aging effects

Finally, we turn to an aging study, using as starting point a sample prepared by mechanical blending, as done in almost all previous studies concerned with mechanical properties of PDMS-silica composites. Substantial aging effects over many months were previously observed by Cohen-Addad and coworkers [16,43] via changes in the swelling behavior and the amount as well as the properties of adsorbed chains (bound-rubber). Here, we use our NMR approach to monitor changes in the bulk samples in real time.

The unprocessed DQ build-up curves plotted in Fig. 6a demonstrate the substantial changes in the network-like behavior in a mechanically mixed sample over months. Even after 5 months, the properties of the analogous solution-blended sample X-15 are not recovered, which also highlights the good efficiency of solution blending in order to obtain optimized composites. Results from the component analysis can be inspected in Fig. 6b, where it is seen that the network fraction f_{net} increases from 20% to around 40% in the studied time range, while the linear-chain signal (chain centers as well as the end fractions) decrease. The residual coupling characterizing the cross-link density of the network fraction also increases, suggesting a successive shortening of the effective network chains, possibly along with a slow re-organization of the sample morphology. The high value around 200 Hz measured for X-15 is not reached, indicating that the particle dispersion in the latter sample is still better (see Fig. 1b).

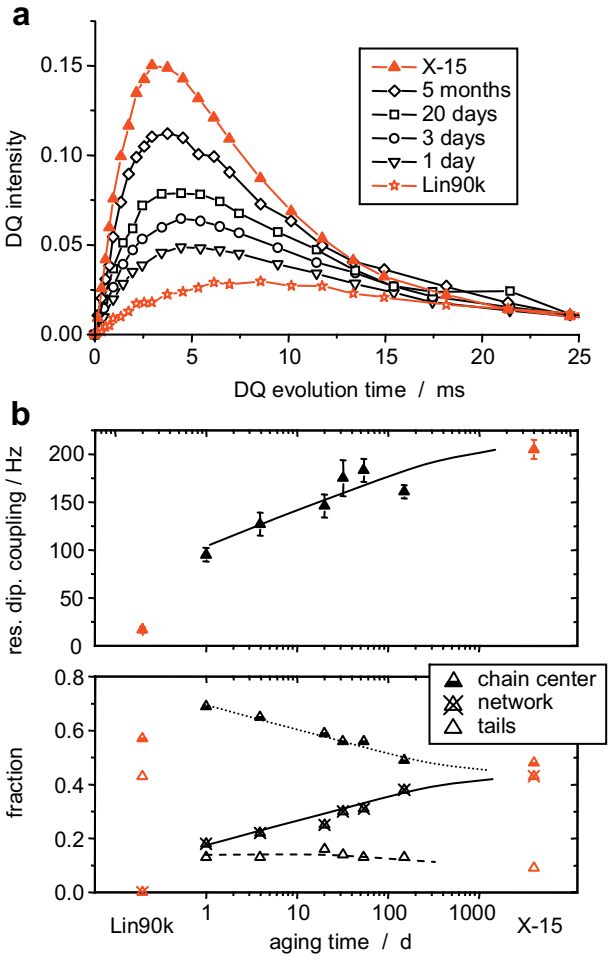

Fig. 6. (a) Time-dependent DQ build-up curves, with intensities relative to the full sample signal, for a sample with 15 wt% unmodified silica prepared by melt blending, as compared to the Lin90k and X-15 data. (b) Results of the component analysis of the same collection of data. The lines are guides to the eye.

4. Conclusions

We have shown that low-field multiple-quantum NMR, combined with a microscopic characterization, and mechanical as well as swelling experiments, provides a consistent picture of the physical network formation in silica-filled PDMS composites without chemical crosslinking, prepared by solution blending. In this system, sections of the chains are strongly adsorbed at the particle surface, forming crosslinks and thus macroscopic networks characterized by entropic elasticity. The NMR signal was deconvoluted into three components, linear-chain centers, rapidly fluctuating tails and a network fraction. The latter, as well as the averaged network chain lengths as deduced from the residual dipolar coupling, were nearly temperature-independent between 250 and 300 K, and correlated well with macroscopic determinations of the relaxed modulus and the degree of swelling.

NMR is still useful when the macroscopic techniques cannot be applied any more, that is, for surface-modified and less efficient filler particles, which do not lead to permanent network formation. In these cases, it was found that the fraction of network material and the effective network chain length change characteristically with the surface treatment, which is thus shown to affect the morphology of the samples. The trends are explained by differences in the agglomerate structures, where for PDMS-functionalized particles, agglomerates were found by TEM to be more compact, thus leading to shorter bridging chains. These particles were less active in the overall network formation than trimethylsilyl-funcionalized ones, most probably due to more unreacted residual surface–OH groups in the latter, while the surface of PDMS-grafted particles is supposedly saturated with an adsorption layer even before blending.

We have observed remarkable characteristic changes in the amount of NMR signal related to freely mobile chain ends, which in linear melts are explained by contour-length fluctuations. Adding silica primarily leads to a substantial decrease in this chain end fraction. We have interpreted this as a decrease in the efficiency of contour-length fluctuations of chains which are fixed at one point and cannot reptate any more, but still do not belong to the elastically active network fraction. This phenomenon deserves closer attention in future experiments on better-defined model systems.

Finally, an aging experiment was performed on a conventional mechanically blended sample, revealing re-organizations in the network structure over many months, in agreement with earlier mechanical and adsorption/extraction experiments. From the point of view of NMR, it was revealed that during this time, the network fraction rises continuously, while the network chain length decreases in parallel, possibly demonstrating changes in the dispersion of primary particles. The aged sample did not approach the high network fraction and high cross-link density exhibited by the analogous sample prepared by solution blending. In all, we believe that this work has provided not only new insights into structure–property correlations in polymeric (nano-) composites, but is also a showcase for the potential of advanced NMR techniques for the characterization of complex heterogeneous systems.

Acknowledgments

Funding of this work was provided by the DFG (SFB 428). We are indebted to Ralf Thomann for taking the cryo-TEM images and to Tony Sánchez-Ferrer for his help with the mechanical experiments. AS acknowledges a Kekulé stipend from the Fonds der Chemischen Industrie.

References

[1] Boonstra B, Cochrane H, Dannenberg E. Reinforcement of silicone rubber by particular silica. Rubber Chem Technol 1970;48:558.
[2] Schmid H, Michel B. Siloxane polymers for high-resolution soft lithography. Macromolecules 2000;33:3042–9.
[3] Cohen-Addad JP, Roby C, Sauviat M. Characterization of chain binding to filler in silicone–silica systems. Polymer 1985;26:1231–3.
[4] Litvinov VM, Zhdanov AA. Molecular motions in filled polydimethylsiloxanes. Vysokomol Soyed A 1987;29:1021–7.
[5] Kirst KU, Kremer F, Litvinov VM. Broad-band dielectric spectroscopy on the molecular dynamics of bulk and adsorbed poly(dimethylsiloxane). Macromolecules 1993;26:975–80.
[6] Litvinov VM, Barthel H, Weis J. Structure of a PDMS layer grafted onto a silica surface studied by means of DSC and solid-state NMR. Macromolecules 2002;35:4356–64.
[7] Maxwell RS, Balazs B, Cohenour R, Prevedel E. Aging of silica-filled PDMS/PDPS copolymers in desiccating environments: a DSC and NMR study. Macromol Symp 2003;202:291–6.
[8] Gee RH, Maxwell RS, Balazs B. Molecular dynamics studies on the effects of water speciation on interfacial structure and dynamics in silica-filled PDMS composites. Polymer 2004;45:3885–91.
[9] Viallat A, Cohen-Addad JP, Pouchelon A. Mechanically induced sorption of siloxane on silica: experimental and theoretical investigations of chain binding, collective behavior and multiple-aggregate processes. Polymer 1986;27:843–8.
[10] Cohen-Addad JP, Viallat A. Nuclear magnetic resonance approach to the characterization of siloxane–silica network-like structures. Polymer 1986;27:1855–63.
[11] Barthel H. Surface interactions of dimethylsiloxy group-modified fumed silica. Colloids Surf A 1995;101:217–26.
[12] Aranguren MI, Mora E, DeGroot Jr JV, Macosko CW. Effect of reinforcing fillers on the rheology of polymer melts. J Rheol 1992;36:1165–82.
[13] Sun G, Butt H-J. Adhesion between solid surfaces in polymer melts: bridging of single chains. Macromolecules 2004;37:6086–9.
[14] Cosgrove T, Turner MJ, Thomas DR. The adsorption of polydimethylsiloxane onto silica from the melt. Polymer 1997;38:3885–92.
[15] Kosinski LE, Caruthers JM. The effect of molecular weight on the rheological properties of poly(dimethylsiloxane) filled with fumed silica. Rheol Acta 1986;25:153–60.
[16] Cohen-Addad JP. Approach to the swelling characterization of silica-filled siloxane systems. Polym Commun 1987;28:121–3.
[17] Cohen-Addad JP. Sol or gel-like behaviour of ideal silica–silicone mixtures: percolation approach. Polymer 1992;33:2762–7.
[18] DeGroot Jr JV, Macosko CW. Aging phenomena in silica-filled polydimethylsiloxane. J Colloid Interface Sci 1999;217:86–93.
[19] Piau J-M, Dorget M, Palierne J-F. Shear elasticity and yield stress of silica–silicone physical gels: fractal approach. J Rheol 1999;43:305–14.
[20] Paquien J-N, Galy J, Gérard J-F, Pouchelon A. Rheological studies of fumed silica–polydimethylsiloxane suspensions. Colloids Surf A 2005;260:165–72.
[21] Shim SE, Isayev AI. Rheology and structure of precipitated silica and poly(-dimethyl siloxane) system. Rheol Acta 2004;43:127–36.
[22] Cohen-Addad JP, Morel N. NMR investigations into polydimethylsiloxane adsorption on silica aggregates. J Phys III France 1996;6:267–77.
[23] Cohen-Addad JP. Effect of the anisotropic chain motion in molten polymers: the solidlike contribution of the nonzero average dipolar coupling to NMR signals. Theoretical description. J Chem Phys. 1974;60:2440–53.
[24] Saalwächter K. Artifacts in transverse proton NMR relaxation studies of elastomers. Macromolecules 2005;38:1508–12.
[25] Garrido L, Mark JE, Sun CC, Ackerman JL, Chang C. NMR characterization of elastomers reinforced with in situ precipitated silica. Macromolecules 1991; 24:4067–72.
[26] Saalwächter K. proton multiple-quantum nmr for the study of chain dynamics and structural constraints in polymeric soft materials. Prog Nucl Magn Reson Spectrosc 2007;51:1–35.
[27] Brebner KI, Chahal RS, St-Pierre LE. Adsorption of poly(diemthyl siloxanes) from solution onto silica: 1. Polymer 1980;21:533–40.
[28] Saalwächter K, Ziegler P, Spyckerelle O, Haidar B, Vidal A, Sommer J-U. ^{1}H multiple-quantum nuclear magnetic resonance investigations of molecular order distributions in poly(dimethylsiloxane) networks: evidence for a linear mixing law in bimodal systems. J Chem Phys 2003;119:3468–82.
[29] Saalwächter K, Gottlieb M, Liu R, Oppermann W. Gelation as studied by proton multiple-quantum NMR. Macromolecules 2007;40:1555–61.
[30] Saalwächter K, Heuer A. Chain dynamics in elastomers as investigated by proton multiple-quantum NMR. Macromolecules 2006;39:3291–303.
[31] Saalwächter K, Herrero B, López-Manchado MA. Chain order and crosslink density of elastomers as investigated by proton multiple-quantum NMR. Macromolecules 2005;38:9650–60.
[32] Graf R, Heuer A, Spiess HW. Chain-order effects in polymer melts probed by ^{1}H double-quantum NMR spectrocopy. Phys Rev Lett 1998;80:5738–41.
[33] Kimmich R, Köpf M, Callaghan P. Components of transverse NMR relaxation in polymer melts: influence of chain-end dynamics. J Polym Sci B Polym Phys 1991;29. 10255–30.
[34] Schillé E, Cohen-Addad J-P, Guillermo A. Concentrated solutions of partly deuterated triblock polybutadiene. Segmental analysis of NMR properties. Macromolecules 2004;37:401–17.

[35] Maus A, Saalwächter K. Crystallization kinetics of poly(dimethylsiloxane) molecular-weight blends — correlation with local chain order in the melt? Macromol Chem Phys 2007;208:2066–75.
[36] Saalwächter K, Sommer J-U. NMR reveals non-distributed and uniform character of network chain dynamics. Macromol Rapid Commun 2007;28: 1455–65.
[37] Saalwächter K, Klüppel M, Luo H, Schneider H. Chain order in filled sbr elastomers: a proton multiple-quantum NMR study. Appl Magn Reson 2004;27: 4071–417.
[38] Milner ST, McLeish TCB. Reptation and contour-length fluctuations in melts of linear polymers. Phys Rev Lett 1998;81:725–8.
[39] Abdel-Goad M, Pyckhout-Hintzen W, Kahle S, Allgaier J, Richter D, Fetters LJ. Rheological properties of 1,4-polyisoprene over a large molecular weight range. Macromolecules 2004;37:8135–44.
[40] Acosta RH, Monti GA, Villar MA, Vallés EM, Vega DA. Transiently trappend entanglements in model polymer networks. Macromolecules 2009;42:4674–80.
[41] Flory PJ. Principles of polymer chemistry. Ithaca: Cornell University Press; 1953.
[42] Peirotti MB, Deiber JA, Ressia JA, Villar MA, Vallés EM. Relaxation modes of molten polydimethylsiloxane. Rheol Acta 1998;37:449–62.
[43] Cohen-Addad JP, Touzet S. Poly(dimethylsiloxane)–silica mixtures: intermediate states of adsorption and swelling properties. Polymer 1993;34:3490–8.